

Systematic investigation of magneto-electronic, structural, thermoelectric and optical properties of Nd_2MgX_4 (X = S, Se) compounds

M. Fida^a, Nasarullah^a, S. A. Aldaghfag^b, M. Yaseen^{a,*}, M. Ishfaq^a

^a*Spin-Optoelectronics and Ferro-Thermoelectric (SOFT) Materials and Devices Laboratory, Department of Physics, University of Agriculture, Faisalabad 38040, Pakistan*

^b*Department of Physics, College of Sciences, Princess Nourah bint Abdulrahman University, P. O. Box 84428, Riyadh 11671, Saudi Arabia*

The structural, magnetic, optoelectronic, and thermoelectric (TE) characteristics of Nd_2MgX_4 (X = S, Se) are determined by utilizing the density functional theory (DFT) based full potential linearized augmented plane wave (FP-LAPW) method as employed in WEIN2k code. The exchange and correlation energies along with Coulomb interactions are brought into consideration by employing local density of approximation with Hubbard model (LDA+U). Tolerance (τ) factor and formation enthalpy were utilized to confirm the stability of both spinels. τ values are 0.70 and 0.68, and formation enthalpy values are (ΔH_f) are -3.34 eV and -2.19 eV for Nd_2MgX_4 (X = S, Se), respectively. For Nd_2MgX_4 (X = S, Se) metallic behavior is found in spin up case while considerable bandgaps are found in spin down with half metallic bandgap (E_g) values of 1.82 and 1.26 eV (in spin down), correspondingly. The calculated magnetic moment for Nd_2MgX_4 (X = S, Se) are 12.0008 μ_B and 12.0003 μ_B , respectively. Furthermore, optical features including refractive index $n(\omega)$, dielectric constant $\epsilon(\omega)$, reflectivity $R(\omega)$, optical conductivity $\sigma(\omega)$, absorption coefficient $\alpha(\omega)$ and extinction coefficient $k(\omega)$ are computed. The maximum calculated real part of dielectric constant $\epsilon_1(\omega)$ values for Nd_2MgX_4 (X = S, Se) are 9.2 and 10.8, respectively. For Nd_2MgX_4 (X = S, Se), $\sigma(\omega)$ has maximum value of 7642.9 at 6.6 and 7592.5 ($\Omega \text{ cm}$)⁻¹ at 5.99 eV, respectively. The various temperature dependent thermoelectric (TE) parameters along with figure of merit (ZT) are determined to get full insight into the TE behavior for both compounds by using BoltzTraP code. The computed ZT value for Nd_2MgSe_4 is 0.81 at 800 K while Nd_2MgS_4 has ZT value of 0.80 at 800 K. Results showed that both spinels have potential in spintronics and in cooling industries.

(Received May 18, 2023; Accepted August 3, 2023)

Keywords: Ferromagnetism, DFT, Spintronics, Spinel

1. Introduction

Spintronics is being helpful for electronic charge and spin in condensed matter physics and has materialized as the fundamental for subsequent generation of digital devices [1]. Magneto-electronics is sub-discipline which deal with such type of devices that make the use of ferromagnetic materials [2]. Recently spinels have attracted a lot of attentions of the researchers due to interesting optical, electrical, magnetic and mechanical properties [3] that play a significant role in a variety of technical applications such as magnetic cores, superconductors[4], data storage, dielectrics, lasers, high-frequency devices[5], different sensors[6], biotechnology and giant magneto resistance [7]. The general formula of spinel compounds is AB_2X_4 , where X is chalcogenides (O, S, or Se), A and B are any cations with 2+ and 3+ oxidation state respectively.

Zanib et al. explained the structural, optoelectronic, and transparent features of spinels MgY_2M_4 (M = S, Se) by utilizing DFT method. The bandgap observed for MgY_2S_4 was 2.687 eV and MgY_2Se_4 had bandgap of 2.020 eV. The calculated ZT values for MgY_2X_4 (X = S, Se) were 0.731 and 0.739, respectively [8]. Tahir et al. reported the opto-electronic and TE characteristics of MgSc_2X_4 (X = S, Se) using DFT. Modified Becke-Johnson (mBJ) potential functional was

* Corresponding author: m.yaseen@uaf.edu.pk
<https://doi.org/10.15251/CL.2023.208.559>

employed to obtain precise E_g of 2.334 and 1.727 eV for MgSc_2S_4 and MgSc_2Se_4 , correspondingly. The calculated E_g indicated that such compounds were suitable in photovoltaics and optoelectronic devices that are operating in UV and visible region [9]. Chaudhry et al. explored optoelectronic and structural features of spinels Sc_2XS_4 ($X = \text{Be, Mg, Zn}$) by employing DFT. The bandgaps (E_g) were calculated as 1.60, 2.30, and 1.62 eV, for Sc_2BeS_4 , Sc_2MgS_4 and Sc_2ZnS_4 , correspondingly and suggested for solar cells and photovoltaic applications. The maximum value of refractive index calculated for Sc_2XS_4 ($X = \text{Be, Mg, Zn}$) were 3.75, 3.22 and 3.49, respectively [10].

In this proposed research work the structural, magneto-optoelectronic, and TE features of Nd_2MgX_4 ($X = \text{S, Se}$) are examined by FP-LAPW method. Materials like Nd_2MgX_4 ($X = \text{S, Se}$) have a strong tendency for high carrier mobilities, acceptable band profiles, and a wide range of applications in optoelectronic devices. Despite these qualities, research on Nd_2MgX_4 ($X = \text{S, Se}$) is minimal, therefore the potential of Nd_2MgX_4 ($X = \text{S, Se}$) can be estimated from the knowledge of thermoelectric (TE), electronic and optical features that reported in this work.

2. Computational details

The FP-LAPW method based WIEN2k package is employed to investigate electronic, magnetic structural, thermoelectric (TE) and optical features of Nd_2MgX_4 ($X = \text{S, Se}$). A unit cell, in FP-LAPW scheme, consists of two parts. The first part consists of the interstitial region whose potential is increased with the help of plane wave orbitals while second part consists of the muffin tin region. Local density of approximation (LDA + U) was used in the investigations [11]. BoltzTraP code is used to compute TE parameters for Nd_2MgX_4 ($X = \text{S, Se}$) by employing the rigid band approximation (RBA) and constant scattering time approximation (CSTA). Structurally cubic nature unit cell of Nd_2MgX_4 ($X = \text{S, Se}$) is found to have (0.5, 0, 0), (0.125, 0.125, 0.125) and (0.25, 0.25, 0.25) Wyckoff positions for Nd, Mg and X ($X = \text{S, Se}$), respectively. $R_{\text{MT}} \times K_{\text{MAX}} = 7$ is set to regulate the plane wave expansion, where R_{MT} is the lowest of all atomic sphere radii while K_{MAX} is the cut-off of the interspatial plane wave having a sampling of 1000 k-points in the part of the Brillouin zone (BZ) [12]. The valance and core state are splitted by cut-off energy having value of $-6.0 R_y$ while the extension of angular momentum inside the MT sphere is set to be $l_{\text{max}} = 10$ [13]. R_{MT} (muffin-tin radius) values used for A, B, and X were 2.5, 2.39 and 2.39, respectively. In order to get self-consistence, total energy convergence is obtained smaller than 10^{-5} hartrees/cells [14].

3. Results and discussions

3.1. Structural properties

Studied sulfo and seleno-spinels Nd_2MgX_4 ($X = \text{S, Se}$) have cubic geometry with space group $\text{Fd}3\text{m}$ (No. 227) (Fig. 1b & d). In this cubic structure, there are 56 atoms in each cell [15]. The atomic locations in primitive cells are described as Nd = (0.5, 0, 0); (Mg = (0.125, 0.125, 0.125) and S/Se = (0.25, 0.25, 0.25). In order to obtain optimized equilibrium crystal structure, total energy must be minimized. Murnaghan's equation is helpful for calculation of the structural optimization of Nd_2MgX_4 ($X = \text{S, Se}$). Murnaghan equation of state [16] is given below.

$$E(V) = E_0 + \left(\frac{9}{16}\right) V_0 B_0 \left\{ \left[\left(\frac{V_0}{V}\right) - 1 \right] B'_0 + \left[\left(\frac{V_0}{V}\right) - 1 \right] \times 2 \left[3 - 2 \left(\frac{V_0}{V}\right) \right] \right\} \quad (1)$$

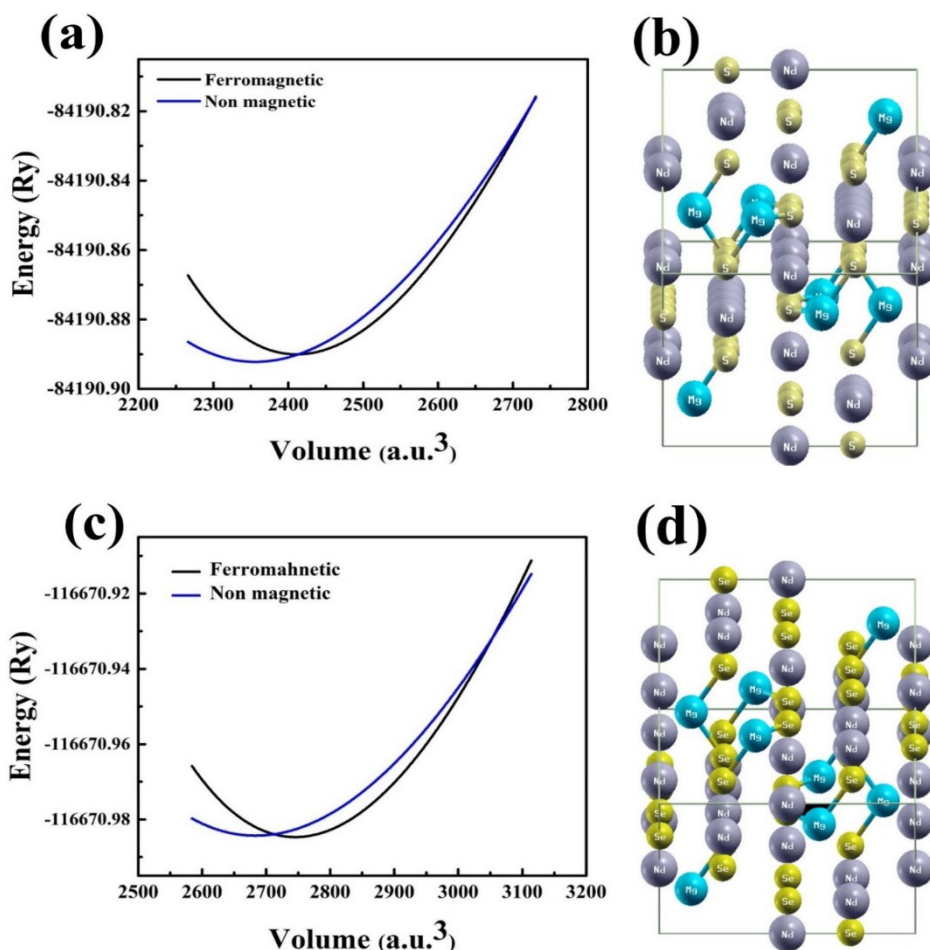


Fig. 1. (a) Optimization and (b) Crystal Structure of Nd_2MgS_4 and (c) Optimization and (d) Crystal Structure of Nd_2MgSe_4 .

The ground state parameters including lattice parameter (\AA), equilibrium energy E_0 (Ry) and volume V_0 (a.u.)³, bulk modulus B_0 (GPa) and its derivative B' with respect to pressure, and enthalpy of formation ΔH_f (eV) are described in Table 1 along with structural parameters reported in previous literature [17], [18]. Bulk modulus (B_0) helps to determine the hardness of material. After replacing sulfur (S) atom with selenium (Se) atom the bulk modulus (B_0) and lattice constant (\AA) show inverse relation [19]. The curve obtained from the energy versus volume is useful to determine optimized lattice constant [20]. The energy versus volume plot of Nd_2MgX_4 ($X = S, Se$) in term of nonmagnetic (NM) and ferromagnetic (FM) is plotted in Fig. 1(a&c).

Formation enthalpy (ΔH_f) is computed to analyze the stability of studied spinels and mathematical expression for ΔH_f is given as [21]

$$\Delta H_f = E_{\text{total}} - lE_{Nd} + mE_{Mg} + nE_X \quad (2)$$

In the above equation E_{total} stands for total formation energy for Nd_2MgX_4 ($X = S, Se$), E_{Nd} , E_{Mg} , and E_X represent the formation energies of respective ions, while l , m and n are number of corresponding ions present per unit cell. The thermal stability for both spinels is demonstrated by negative values of ΔH_f [22]. The computed ΔH_f for Nd_2MgS_4 is -3.34 eV and for Nd_2MgSe_4 is -2.19 eV. Formation energies indicate that the thermal stability decreased from S_4 to Se_4 because ionic radii change from S_4 to Se_4 . Also, tolerance factor (τ) is computed to examine the structural stability of spinels and if τ values lies close to unity the material is said to be structurally stable. It can be determined by using following formula.

$$\tau = \frac{\sqrt{3}(R_B+R_X)}{2(R_A+R_X)} \quad (3)$$

From above relation, R represents the corresponding ionic radii. The calculated τ for Nd_2MgS_4 and Nd_2MgSe_4 are 0.88 and 0.86, respectively (see Table 1). As the values are nearly close to unity, both spinels are structurally stable.

Table 1. Computed M_{TOT} per Co atom (μ_B), interstitial magnetic moments and atomic magnetic moment of each site for $\text{BaTi}_{1-x}\text{Co}_x\text{O}_3$.

Current Study (LDA+U)			PBEsol+GGA [17]		Others [18]	
Parameters	Nd_2MgS_4	Nd_2MgSe_4	Nd_2MgS_4	Nd_2MgSe_4	Nd_2MgS_4	Nd_2MgSe_4
Lattice constant in Å	11.2641	11.7624	11.22	11.73	11.48	12.00
Bulk modulus B_0 (Gpa)	67.0956	53.2243	64.25	55.39		
B'	5.6292	3.8140				
Tolerance factor (τ)	0.88	0.86				
Volume (a.u) ³	2411.1935	2745.5472				
Ground state energy E_0 (Ry)	-84190.89	-11670.98				
ΔH_f (eV)	-3.34	-2.19	-1.82	-1.22	-2.18	-1.65

3.2. Electronic and magnetic properties

Electronic nature has significant impact on other physical characteristics including optical and thermoelectric features so electronic behavior is necessary to compute [23]. To discover the electronic characteristics, the band structures (BS) of Nd_2MgS_4 and Nd_2MgSe_4 along highly symmetric path W-L- Γ -X-W-K and density of states (DOS) have been computed (see Fig.2-4). The dotted line (Fermi level) in band structures and DOS plots separating the conduction band (CB) and valence band (VB). In BS, both Nd_2MgS_4 and Nd_2MgSe_4 show metallicity in spin up and semiconductive gap in the down spin configuration with bandgap of 1.82 and 1.26 eV, correspondingly. It is noted that the incorporation of Se in place of S anion in studied spinels results in decrementing the half metallic bandgap.

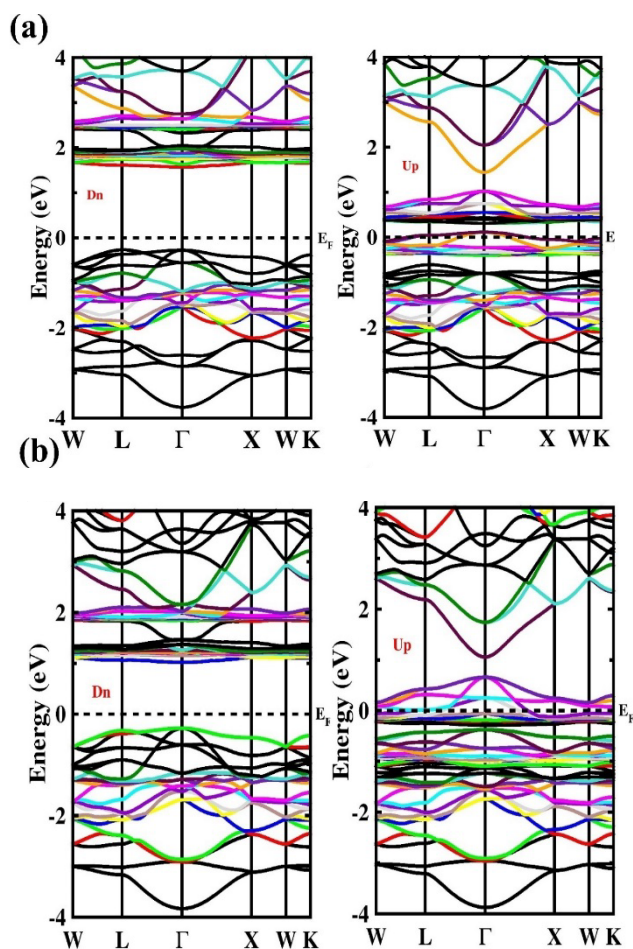


Fig. 2. Calculated BS for cubic Nd_2MgX_4 ($X = S, Se$).

To understand the BS completely, it is necessary to compute total (T) and partial (P) DOS. The spectra of TDOS and PDOS are drawn against energy range of -4 and 4 eV (Figs. 3 & 4). TDOS behavior of Nd_2MgS_4 shows that in spin up channel Mg and S elemental states are responsible for making it half-metallic ferromagnetic (HMF) while Nd_2MgSe_4 is HMF due to elemental states of Mg and Se. Dispersive bands foster from Nd-f and S-p states due to their delocalized nature. More dispersion was seen in VB than CB (see Fig. 4). In the PDOS spectrum of Nd_2MgX_4 ($X = S, Se$) VB is mostly contributed by Nd-f and S-p states and CB is filled by Se-p and Nd-d orbitals with minor influence from Mg-p and S-p orbitals in both spins.

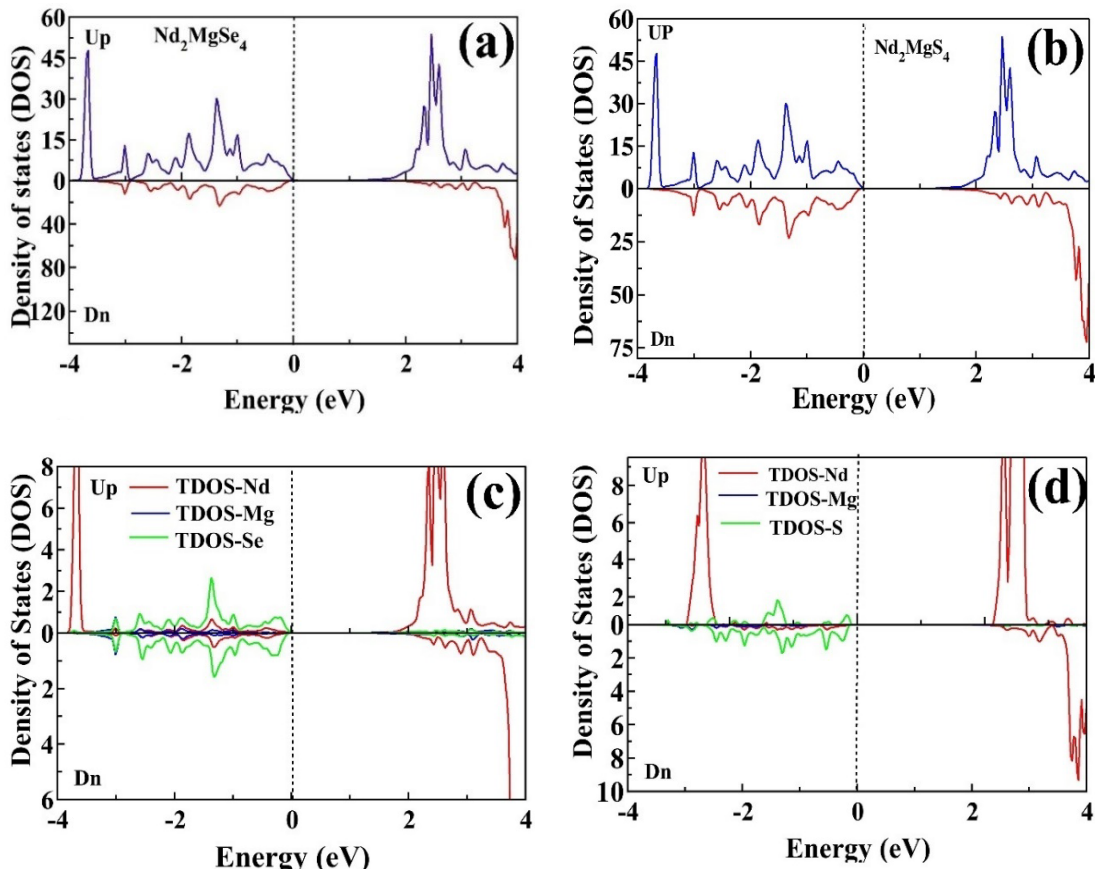


Fig. 3. TDOS of Nd_2MgSe_4 (left) and Nd_2MgS_4 (right).

The magnetic characteristics are examined by partial and total magnetic moments (μ_B). Magnetic spinels based on rare earth cations are considered very interesting and crucial to study because they majorly influence the magnetic moment. The interstitial sites are helpful for confirmation of magnetic moment [24]. The positive and negative values of μ_B are helpful to describe the spin alignment. The spin orientation of cations along the same direction is due to positive sign of magnetic moment and anti-ferromagnetic or ferrimagnetic interaction is described by negative sign[25]. The computed values of interstitial, local, and total magnetic moment of Nd, Se, S and Mg are summarized in Table 2.

Table 2. The calculated value of magnetic moment for Nd_2MgX_4 ($X = S, Se$).

Spinel	Total (μ_B)	Int. (μ_B)	Mg (μ_B)	Nd (μ_B)	S/Se (μ_B)
Nd_2MgS_4	12.0008	0.2629	-0.0029	3.0003	-0.0328
Nd_2MgSe_4	12.0003	0.2439	-0.0045	3.0032	-0.0309
Others [17]					
Nd_2MgS_4	3.000	0.2722	0.0026	2.9066	0.012
Nd_2MgSe_4	3.000	0.2815	0.0017	2.9053	0.011

Nd_2MgS_4 and Nd_2MgSe_4 have μ_B of 12.0008 μ_B and 12.0003 μ_B , correspondingly. The integer values of this μ_B confirm the stable and robust ferromagnetism (FM) of both spinels. The μ_B of Nd_2MgS_4 is greater than Nd_2MgSe_4 . The Nd atom is majorly contributing for total magnetic moment in both compounds. Total μ_B for S and Se_4 encourages parallel μ_B alignment and Mg favors antiparallel μ_B alignment. Nd has a major contribution while Mg and S/Se have minor contribution in total μ_B .

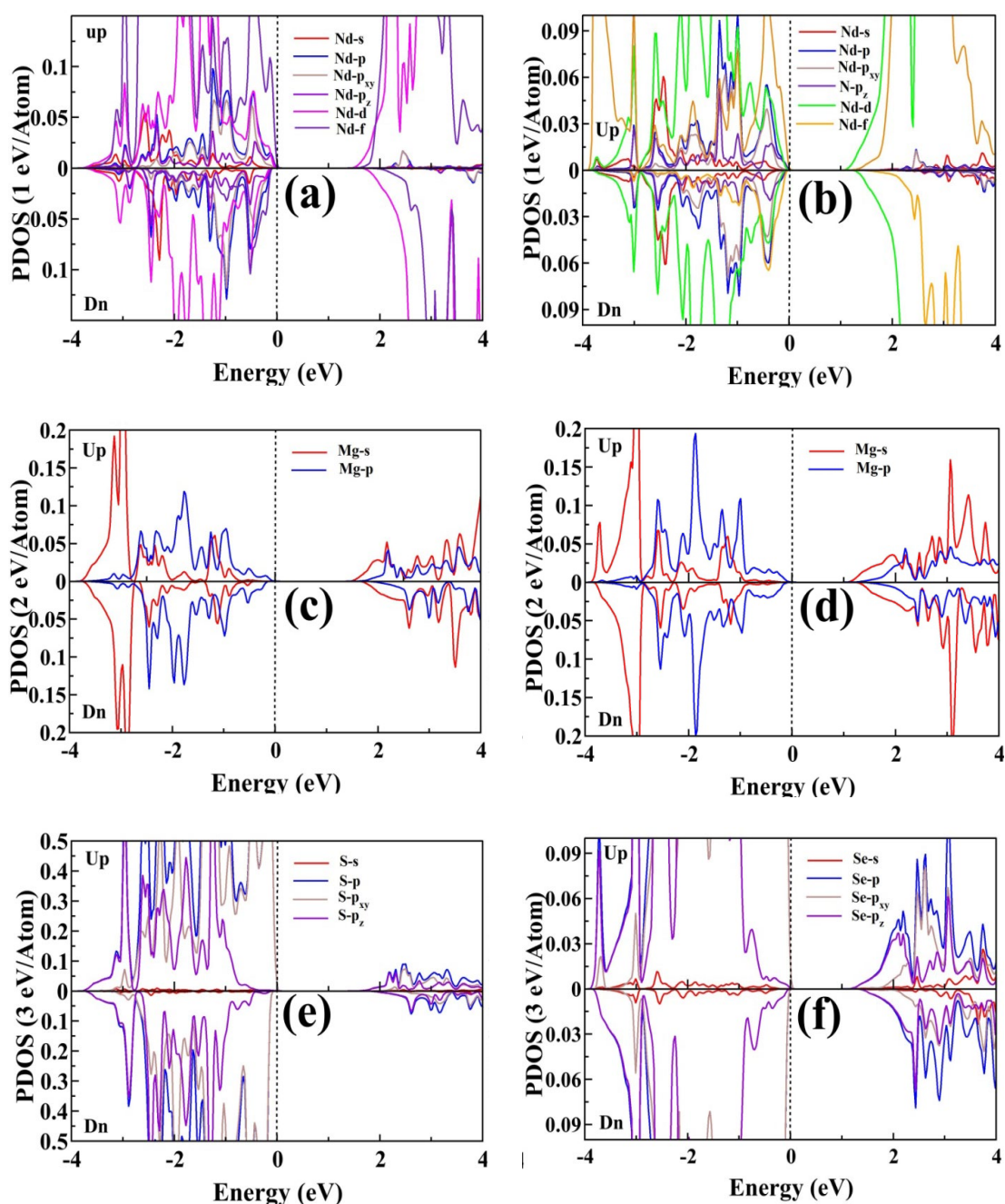


Fig. 4. PDOS of Nd_2MgS_4 (left) and Nd_2MgSe_4 (right).

3.2. Optical properties

Optical characteristics of a compound are related to its response to the incident light and transfer of electrons in different states. Different optical spectra including reflectivity $R(\omega)$, dielectric function $\epsilon(\omega)$, optical conductivity $\sigma(\omega)$, refractive index $n(\omega)$, absorption coefficient $\alpha(\omega)$ and extinction coefficient $k(\omega)$ for Nd_2MgX_4 ($X=\text{S}, \text{Se}$) are plotted at 0-10 eV (see Fig. 5-6). Dielectric function $\epsilon(\omega)$ is explained in terms of real $\epsilon_1(\omega)$ and imaginary $\epsilon_2(\omega)$ parts, i.e., $\epsilon(\omega) = \epsilon_1(\omega) + i\epsilon_2(\omega)$ [26]. Material polarization and absorption are portrayed by $\epsilon_1(\omega)$ and $\epsilon_2(\omega)$, respectively [27]. $\epsilon_1(\omega)$ is calculated by using $\epsilon_2(\omega)$ by solving Kramers-Kronig equation [28] as given

$$\varepsilon_1(\omega) = 1 + \frac{2}{\pi} p \int_0^{\theta} \frac{\omega' \varepsilon_2(\omega')}{\omega'^2 - \omega^2} d\omega' \quad (4)$$

where p is a Cauchy Principle value. The calculated value of static real part $\varepsilon_1(0)$ for Nd_2MgS_4 and Nd_2MgSe_4 are 6.15 and 6.95, respectively while peak is obtained at 2.5 eV for Nd_2MgS_4 and at 2.3 eV for Nd_2MgSe_4 . The calculated $\varepsilon_1(\omega)$ values reveal that while replacing anion S with Se then the value of $\varepsilon_1(\omega)$ increases from 6.15 to 6.95 (depicted in Fig. 5(a)). Additionally, the mathematical expression which relates $\varepsilon_1(\omega)$ and E_g is termed as Penn's Model and is given below [29].

$$\varepsilon_1(0) = 1 + \left(\frac{\hbar \omega_p}{E_g} \right)^2 \quad (5)$$

The $\varepsilon_2(\omega)$ shows the absorptive behavior for the materials. The maximum peak of $\varepsilon_2(\omega)$ for Nd_2MgS_4 and Nd_2MgSe_4 appears at 6.2 and 5.7 eV, respectively (see Fig. 5(b)). Material transparency is explained by $n(\omega)$ when light is incident on a surface of a compound [30]. Following equation is solved to calculate the $n(\omega)$ [31].

$$n(\omega) = \frac{1}{\sqrt{2}} [\{\varepsilon_1(\omega)^2 + \varepsilon_2(\omega)^2\}^{\frac{1}{2}} + \varepsilon_1(\omega)]^{1/2} \quad (6)$$

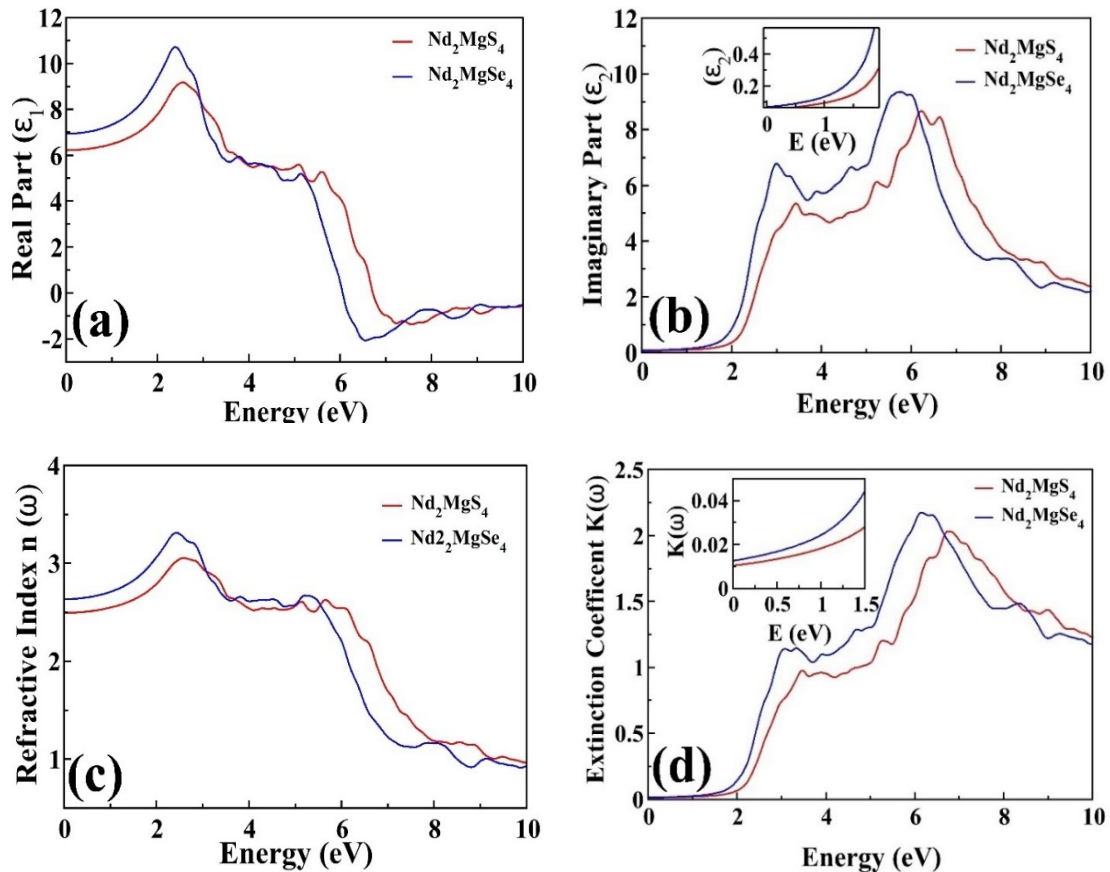


Fig. 5. (a) $\varepsilon_1(\omega)$, (b) $\varepsilon_2(\omega)$, (c) $n(\omega)$ and (d) $k(\omega)$ of Nd_2MgX_4 ($X = \text{S}, \text{Se}$).

The calculated static $n(\omega)$ values (at 0 eV) for Nd_2MgS_4 and Nd_2MgSe_4 are 2.5 and 2.6, correspondingly, while Nd_2MgS_4 shows extreme $n(\omega)$ value of 3.1 at 2.6 eV and Nd_2MgSe_4 shows extreme $n(\omega)$ value of 3.4 at 2.4 eV (see Fig. 5(c)). $\varepsilon_1(\omega)$ and $n(\omega)$ are associated together by the relation $\varepsilon_1(\omega) = n^2 - k^2$ [25]. When EM waves travel through a substance, the quantity $k(\omega)$ describes how much light is absorbed during that process [32]. $k(\omega)$ peak value of 2.1 appears at 6.7 eV for Nd_2MgS_4 while for Nd_2MgSe_4 it has highest value of 2.2 at 6.1 eV (see Fig. 5(d)).

Absorption coefficient $\alpha(\omega)$ measures the absorption energy of electromagnetic (EM) wave [33]. A linear behavior with little fluctuations is observed for both compounds and the peak for Nd_2MgS_4 is found to be $143.16 (10^4/\text{cm})$ at 8.6 while for Nd_2MgSe_4 , it is $143.16 (10^4/\text{cm})$ at 6.4 eV (Fig. 6a).

The findings demonstrate that both spinels are viable options for photovoltaics. Conductivity influenced by transport of electrons which jump towards CB in response to incident light can be termed as optical conductivity $\sigma(\omega)$ [34]. Highest value of $\sigma(\omega)$ is found to be $7642.9 (\Omega \text{ cm})^{-1}$ at 6.6 eV while Nd_2MgSe_4 has first highest peak value of $7592.5 (\Omega \text{ cm})^{-1}$ at 5.99 eV (Fig. 6b). The spectrum of $\sigma(\omega)$ is same as that of $\epsilon_2(\omega)$ and $k(\omega)$.

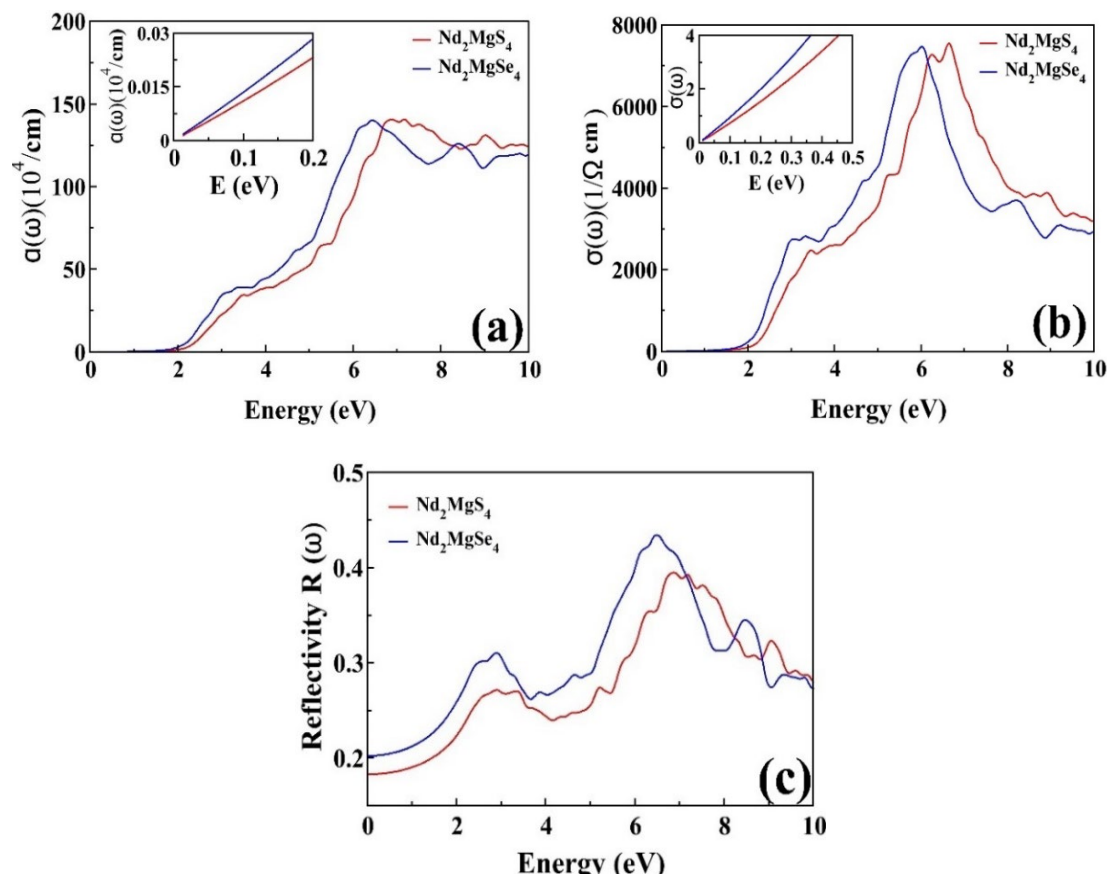


Fig. 6. (a) $\alpha(\omega)$, (b) $\sigma(\omega)$ and (c) $R(\omega)$ of Nd_2MgX_4 ($X = \text{S}, \text{Se}$).

$R(\omega)$ is the measure of the tendency of a material to reflect the incoming photons and mathematically can be expressed as [35].

$$R = \left| \frac{n'-1}{n'+1} \right|^2 = \frac{(n(\omega)-1)^2 + k^2(\omega)}{(n(\omega)+1)^2 + k^2(\omega)} \quad (7)$$

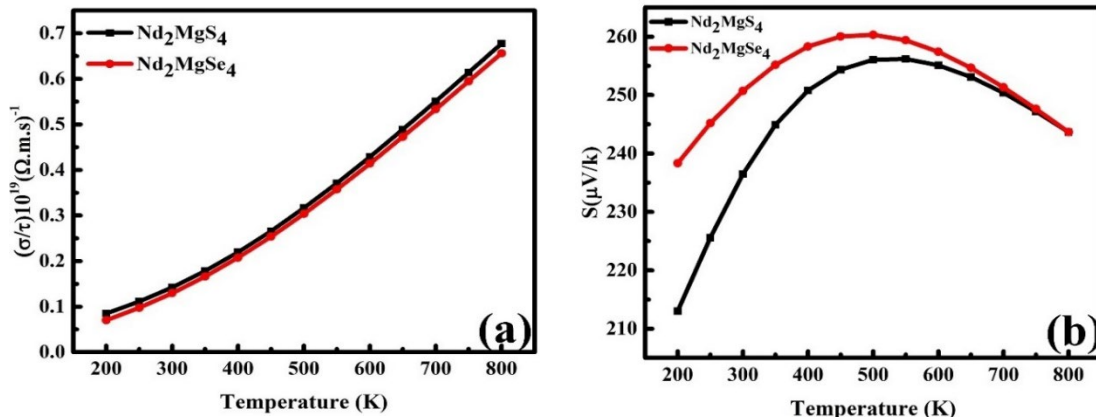
The computed $R(\omega)$ value for Nd_2MgS_4 is 0.18 at 0 eV while the uppermost peak appears as 0.39 at 6.9 eV. The $R(\omega)$ value for Nd_2MgSe_4 is 0.21 at 0 eV and has the extreme value 0.44 at 6.4 eV (Fig. 6c). The calculated optical parameter values are tabulated below.

Table 3. The computed value of optical parameters for Nd_2MgX_4 ($X= S, Se$).

Optical parameters	Present Study		Existed Data [17]	
	Nd_2MgS_4	Nd_2MgSe_4	Nd_2MgS_4	Nd_2MgSe_4
$\epsilon_1(0)$	6.15	6.95	5.24	5.99
$n(0)$	2.5	2.6	2.29	2.45
$R(0)$	0.18	0.21	0.15	0.18

3.3. Thermoelectric properties

Thermoelectric (TE) properties are crucial and are frequently employed to address energy crises [36]. The study of spinel chalcogens are getting more interest by the researchers because of the valuable usage in TE material [37]. By applying relaxation time within the BoltzTraP code, TE parameters like σ/τ , S , k/τ , PF, and ZT have been investigated. A material that has the greatest value of ZT is suitable for the working of TE devices, such a highest value related to low k/τ , and higher σ/τ and S values [38]. The σ/τ is directly related to temperature and carrier concentration [39]. Initially, linear increasing behavior is observed with the rise of temperature for both spinels and the highest value of σ/τ for Nd_2MgS_4 and Nd_2MgSe_4 are 0.68 and 0.65 $(\Omega.m.s)^{-1}$, correspondingly at 800 K (see Fig. 7(a)).

Fig. 7 The calculated values of (a) σ/τ (b) S , (c) k/τ and (d) PF of Nd_2MgX_4 ($X= S, Se$).

S can be obtained by dividing the potential difference to a gradient temperature i.e $S=\Delta V/\Delta T$ [40]. S values for both compounds initially rise with temperature increase, but after 500 K, values of S fall with temperature increases and the highest values of S are 255 and 260 $\mu V/k$ for Nd_2MgS_4 and Nd_2MgSe_4 , respectively (see Fig. 7(b)). Both positive S value indicate the holes as majority carriers (p-type) while n-type bandgap materials give negative S values [41]. The current investigation exhibits positive values of S , indicating that the major carriers are holes (p-type). Nd_2MgSe_4 has higher S values than Nd_2MgS_4 which can be attributed to the lower bandgap of former spinel. Another important TE phenomenon is thermal conductivity (k/τ) which determines heat flows [42] and it is sum of parts of phononic k_{ph} and electronic k_e sections [43]. It is expressed mathematically as $k = k_e + k_{ph}$, from which k_e is electrons mediated heat conduction parameter while k_{ph} is phonons-based heat conduction [44]. Because of low phononic thermal conductivity at high temperatures, only k_e is computed. The k_e/τ gradually rises with increase of temperature (see Fig. 7(c)). The maximum calculated value of k/τ for Nd_2MgS_4 and Nd_2MgSe_4 are 3.9 and 4 W/mKs, respectively at temperature of 800 K.

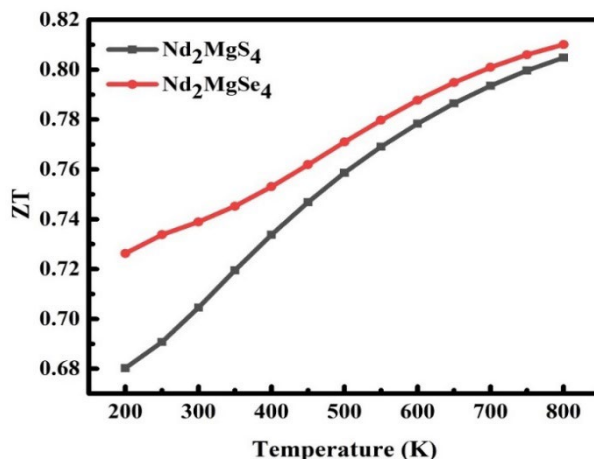


Fig. 8. ZT for Nd_2MgX_4 ($X = S, Se$).

PF is obtained by square of S and electrical conductivity ($PF=S^2\sigma/\tau$) [45]. PF is gradually increased with the rise of temperature and both Nd_2MgS_4 and Nd_2MgSe_4 have highest values of PF of 4.1 and 3.9 W/mK^2s , respectively at 800 K (see Fig. 7(d)). ZT is computed to understand effectiveness of studied spinels for TE applications. ZT can be written as [46]

$$ZT = \frac{S^2\sigma T}{k} \quad (8)$$

The maximum calculated values of ZT for Nd_2MgS_4 and Nd_2MgSe_4 are 0.80 and 0.81, respectively at 800 K temperature (see Fig. 8). As ZT values are approaching unity which serves as a standard for TE device efficiency [47]. Furthermore, all the thermoelectric parameter values at 800 K temperature are listed in Table 4. Presented analysis shows that both suggested spinels Nd_2MgS_4 and Nd_2MgSe_4 are highly desirable for TE devices.

Table 4. TE parameters of Nd_2MgX_4 ($X = S, Se$) at 800 K.

Spinels	(σ/τ) $\times 10^{19}(\Omega.m.s)^{-1}$	Seebeck coefficient ($\mu V/k$)	$(k/\tau)\times 10^{14}$ (W/mKs)	$PF(\sigma S^2)\times 10^{11}$ (W/mK^2s)	ZT
Nd_2MgS_4	0.68	255	3.9	4.1	0.8
Nd_2MgSe_4	0.65	260	4	3.9	0.81

4. Conclusion

The first principles based DFT within WEIN2k code is employed to analyze the structural, magneto-optoelectronic, and TE properties of Nd_2MgX_4 ($X = S, Se$). The calculated half metallic gaps for Nd_2MgX_4 ($X = S, Se$) are 1.82 and 1.26 eV (spin down). The calculated lattice constants for optimized Nd_2MgX_4 ($X = S, Se$) structures are 11.2642 Å and 11.7624 Å, respectively. Both spinels Nd_2MgS_4 and Nd_2MgSe_4 are half metallic ferromagnets having integer magnetic moments: 12.0008 μB and 12.0003 μB , correspondingly. For Nd_2MgS_4 and Nd_2MgSe_4 , the static $n(\omega)$ calculated to be 2.5 and 2.6, respectively. The optical absorption peak is determined to be 143.16 ($10^{14}/cm$) at 8.6 eV for Nd_2MgS_4 and 143.16 ($10^{14}/cm$) at 6.4 eV for Nd_2MgSe_4 . The calculated value of ZT for Nd_2MgX_4 ($X=S, Se$) are 0.80 and 0.81, respectively at 800 K. Findings show that both spinels are promising applicants for optoelectronics and TE coolers.

Acknowledgements

The authors express their gratitude to Princess Nourah bint Abdulrahman University Researchers Supporting Project number (PNURSP2023R81), Princess Nourah bint Abdulrahman University, Riyadh , Saudi Arabia.

References

- [1] D. Santos-Carballal, A. Roldan, R. Grau-Crespo, N.H. De Leeuw, *Physical Review B - Condensed Matter and Materials Physics*. 91, 1-13 (2015).
- [2] C. Felser, G.H. Fecher, B. Balke, *Angewandte Chemie - International Edition*. 46, 668-699 (2007); <https://doi.org/10.1002/anie.200601815>
- [3] A. Hossain, M.S.I. Sarker, M.K.R. Khan, M.M. Rahman, *Materials Science and Engineering B: Solid-State Materials for Advanced Technology*. 253, 114496 (2020); <https://doi.org/10.1016/j.mseb.2020.114496>
- [4] F. Zerarga, A. Bouhemadou, R. Khenata, S. Bin-Omran, *Solid State Sciences*. 13, 1638-1648 (2011); <https://doi.org/10.1016/j.solidstatesciences.2011.06.016>
- [5] G. Pilania, V. Kocevski, J.A. Valdez, C.R. Kreller, B.P. Uberuaga, *Communications Materials*. 1, 1-11 (2020); <https://doi.org/10.1038/s43246-020-00082-2>
- [6] V.S. Zhandun, A. Nemtsev, *Journal of Magnetism and Magnetic Materials*. 499, 166306 (2020); <https://doi.org/10.1016/j.jmmm.2019.166306>
- [7] M.U. Sohaib, K. Abid, N.A. Noor, M.A. Khan, R. Neffati, S.H. Abdel-hafez, E.E. Hussein, *Journal of Materials Research and Technology*. 15, 4683-4693 (2021); <https://doi.org/10.1016/j.jmrt.2021.10.057>
- [8] M. Zanib, N.A. Noor, M.A. Iqbal, I. Mahmood, A. Mahmood, S.M. Ramay, N.Y.A. Al-Garadi, T. Uzzaman, *Current Applied Physics*. 20, 1097-1102 (2020); <https://doi.org/10.1016/j.cap.2020.07.003>
- [9] W. Tahir, G.M. Mustafa, N.A. Noor, S.M. Alay-e-Abbas, Q. Mahmood, A. Laref, *Ceramics International*. 46, 26637-26645 (2020); <https://doi.org/10.1016/j.ceramint.2020.07.133>
- [10] A.R. Chaudhry, B. Ul Haq, S. AlFaify, A. Shaari, A. Laref, *Mater Sci Semicond Process*. 121, 105435 (2021); <https://doi.org/10.1016/j.mssp.2020.105435>
- [11] M.C. Idris, A. Shaari, R. Razali, A. Lawal, S.T. Ahams, *Materials Research Express*, 7, 026304 (2020); <https://doi.org/10.1088/2053-1591/ab7619>
- [12] A. Sohail, S. A. Aldaghfag, M. K. Butt, M. Zahid, M. Yaseen, J. Iqbal, Misbah, M. Ishfaq, A. Dahshan, *Journal of Ovonic Research*, 17(5), 461-469 (2021).
- [13] H. Shafique, S. A. Aldaghfag, M. Kashif, M. Zahid, M. Yaseen, J. Iqbal, Misbah, R. Neffati, *Chalcogenide Letters*, 18(10), 589-599 (2021).
- [14] S.K. Pandey, *Physical Review B*, 86, 085103 (2012); <https://doi.org/10.1103/PhysRevB.86.085103>
- [15] M.I. Kholil, M.T.H. Bhuiyan, *Results in Physics*. 12, 73-82 (2019); <https://doi.org/10.1016/j.rinp.2018.11.026>
- [16] H. Yakhou, A. Maachou, H. Riane, M. Sahnoun, *Computational Condensed Matter*. 21, e00417 (2019); <https://doi.org/10.1016/j.cocom.2019.e00417>
- [17] M. Robail, N.A. Noor, M.W. Iqbal, H. Ullah, A. Mahmood, M.A. Naeem, Y.H. Shin, *Ceramics International*. 48, (2022) 2385-2393; <https://doi.org/10.1016/j.ceramint.2021.10.019>
- [18] A. Jain, S.P. Ong, G. Hautier, W. Chen, W.D. Richards, S. Dacek, S. Cholia, D. Gunter, D. Skinner, G. Ceder, K.A. Persson, *APL Materials*. 1, 011002 (2013); <https://doi.org/10.1063/1.4812323>
- [19] H.A. Alburaih, *Journal of Alloys and Compounds*. 876, 159806 (2021); <https://doi.org/10.1016/j.jallcom.2021.159806>
- [20] M. Rashid, Z. Abbas, M. Yaseen, Q. Afzal, A. Mahmood, S.M. Ramay, *Journal of*

- Superconductivity and Novel Magnetism. 30, 3129-3136 (2017); <https://doi.org/10.1007/s10948-017-4099-0>
- [21] A. Mahmood, M. Rashid, K. Safder, M. Waqas Iqbal, N.A. Noor, S.M. Ramay, W. Al-Masry, N.Y.A. Al-Garadi, Results in Physics. 20, 103709 (2021); <https://doi.org/10.1016/j.rinp.2020.103709>
- [22] Nasarullah, M. Yaseen, S.A. Aldaghfag, M. Zahid, Misbah, Mater Sci Semicond Process. 147, 106760 (2022); <https://doi.org/10.1016/j.mssp.2022.106760>
- [23] M.A. Lahmer, Computational Condensed Matter. 20, e00387 (2019); <https://doi.org/10.1016/j.cocom.2019.e00387>
- [24] M. Khalid, M.W. Iqbal, M. Asghar, N.A. Noor, G.M. Mustafa, S.M. Ramay, European Physical Journal Plus. 137, 59(1-11) (2022); <https://doi.org/10.1140/epjp/s13360-021-02218-w>
- [25] M.K. Butt, M. Yaseen, I.A. Bhatti, J. Iqbal, Misbah, A. Murtaza, M. Iqbal, M. mana AL-Anazy, M.H. Alhossainy, A. Laref, Journal of Materials Research and Technology. 9, 16488-16496 (2020); <https://doi.org/10.1016/j.jmrt.2020.11.055>
- [26] M. mana Al-anazy, T. Zelai, A. Rahim, A.A. AlObaid, T.I. Al-Muhimeed, A.I. Aljameel, A. Mera, A. Dahshan, Q. Mahmood, G. Murtaza, G. Nazir, Journal of Solid State Chemistry. 303, 122480 (2021); <https://doi.org/10.1016/j.jssc.2021.122480>
- [27] S. Al-Qaisi, D.P. Rai, T. Alshahrani, R. Ahmed, B.U. Haq, S.A. Tahir, M. Khuili, Q. Mahmood, Mater Sci Semicond Process. 128, 105766 (2021); <https://doi.org/10.1016/j.mssp.2021.105766>
- [28] K.D. Pham, M. Batouche, D.E.S. Mohammed, T. Seddik, T. V. Vu, D.D. Vo, N.N. Hieu, O.Y. Khyzhun, Journal of Solid State Chemistry. 293, 121763 (2021); <https://doi.org/10.1016/j.jssc.2020.121763>
- [29] D.R. Penn, Phys Rev B. 128(5), 2093-2097 (1962); <https://doi.org/10.1103/PhysRev.128.2093>
- [30] M. Nazar, Nasarullah, S.A. Aldaghfag, M. Yaseen, M. Ishfaq, R.A. Khera, S. Noreen, M.H. Abdellattif, Journal of Physics and Chemistry of Solids. 166, 110719 (2022); <https://doi.org/10.1016/j.jpcs.2022.110719>
- [31] M.A. Rafiq, A. Javed, M.N. Rasul, M.A. Khan, A. Hussain, Ceramics International. 46, 4976-4983 (2020); <https://doi.org/10.1016/j.ceramint.2019.10.237>
- [32] I.M. Chiromawa, A. Shaari, R. Razali, L.S. Taura, A. Lawal, Materials Today Communications. 25, 101665 (2020); <https://doi.org/10.1016/j.mtcomm.2020.101665>
- [33] M. Reffas, A. Bouhemadou, R. Khenata, T. Ouahrani, S. Bin-Omran, Physica B: Condensed Matter. 405, 4079-4085 (2010); <https://doi.org/10.1016/j.physb.2010.06.058>
- [34] S.J. Moon, M.W. Kim, K.W. Kim, Y.S. Lee, J.Y. Kim, J.H. Park, B.J. Kim, S.J. Oh, S. Nakatsuji, Y. Maeno, I. Nagai, S.I. Ikeda, G. Cao, T.W. Noh, Phys Rev B Condens Matter Mater Phys. 74, 113104 (2006).
- [35] A. Aziz, S.A. Aldaghfag, M. Zahid, J. Iqbal, Misbah, M. Yaseen, H.H. Smailly, Physica B: Condensed Matter. 630, 413694 (2022); <https://doi.org/10.1016/j.physb.2022.413694>
- [36] G.M. Mustafa, T. Zelai, S. Bouzgarrou, M.H. Alhossainy, Q. Mahmood, A. Mera, H.H. Hegazy, S. Alharthi, M.A. Amin, Applied Physics A: Materials Science and Processing. 128, 38(1-10) (2022); <https://doi.org/10.1007/s00339-021-05152-x>
- [37] N.A. Noor, M. Rashid, G.M. Mustafa, A. Mahmood, W. Al-Masry, S.M. Ramay, Journal of Alloys and Compounds. 856, 157198 (2021); <https://doi.org/10.1016/j.jallcom.2020.157198>
- [38] Q. Mahmood, B. Ul Haq, M. Rashid, N.A. Noor, S. AlFaify, A. Laref, Journal of Solid State Chemistry. 286, 121279 (2020); <https://doi.org/10.1016/j.jssc.2020.121279>
- [39] M. Saeed, Z. Noor, R. Ali, A. Laref, H.M. Althib, T.H. Flemban, G. Murtaza, International Journal of Energy Research. 45, 8307-8315 (2021); <https://doi.org/10.1002/er.6504>
- [40] S. Ali, M. Rashid, M. Hassan, N.A. Noor, Q. Mahmood, A. Laref, B.U. Haq, Physica B: Condensed Matter. 537, 329-335 (2018); <https://doi.org/10.1016/j.physb.2018.02.039>
- [41] T. Ghrib, A. Rached, E. Algrafy, I.A. Al-nauim, H. Albalawi, M.G.B. Ashiq, B.U. Haq, Q. Mahmood, Materials Chemistry and Physics. 264, 124435 (2021);

<https://doi.org/10.1016/j.matchemphys.2021.124435>

[42] M. Tariq, M.A. Ali, A. Laref, G. Murtaza, Solid State Communications. 314-315 113929 (2020); <https://doi.org/10.1016/j.ssc.2020.113929>

[43] M. Waseem, I. Mahmood, M. Rashid, I. Qasim, A. Laref, Physics Letters, Section A: General, Atomic and Solid State Physics. 383, 1810-1815 (2019);
<https://doi.org/10.1016/j.physleta.2019.02.048>

[44] B. Ul Haq, R. Ahmed, S. AlFaify, F.K. Butt, A. Shaari, A. Laref, Intermetallics. 93, 235-243 (2018); <https://doi.org/10.1016/j.intermet.2017.09.017>

[45] F. Zareef, M. Rashid, A.A.H. Ahmadini, T. Alshahrani, N.A. Kattan, A. Laref, Mater Sci Semicond Process. 127, 105695 (2021); <https://doi.org/10.1016/j.mssp.2021.105695>

[46] F. Majid, M.T. Nasir, E. Algrafy, M. Sajjad, N.A. Noor, A. Mahmood, S.M. Ramay, Journal of Materials Research and Technology. 9, 6135-6142 (2020);
<https://doi.org/10.1016/j.jmrt.2020.04.016>

[47] M. Zafarullah, M. Ishfaq, S.A. Aldaghfag, M. Yaseen, M. Zahid, M. Nazar, R. Neffati, J Magn Magn Mater. 560, 169657 (2022); <https://doi.org/10.1016/j.jmmm.2022.169657>